The spin-1 Lai - Sutherland model with external and internal fields: I. The phase diagram

1996 J. Phys. A: Math. Gen. 29 3951

(http://iopscience.iop.org/0305-4470/29/14/019)

J. Phys. A: Math. Gen. **29** (1996) 3951–3962. Printed in the UK

The spin-1 Lai–Sutherland model with external and internal fields: I. The phase diagram

A Schmitt†§, K-H Mütter†‖ and M Karbach‡¶+

† Physics Department, University of Wuppertal, D-42097 Wuppertal, Germany
‡ Department of Physics, The University of Rhode Island, Kingston, RI 02881, USA

Received 26 February 1996

Abstract. The one-dimensional $S = 1$ quantum spin chain with a linear and bilinear nearest-neighbour interaction of equal strength is integrable by the nested Bethe ansatz. In this paper the model is studied in the presence of an external magnetic field and an internal crystal field. By solving the Bethe ansatz equations for chains up to length $N = 360$ we construct the complete phase diagram of the system. We discuss how the magnetization curves depend on the internal field. In the $SU(3)$ phase, where all three densities of atoms with S_3-component -1, 0, $+1$ are non-vanishing, lines of constant density can be approximately parametrized by modified hypocycloides.

1. Introduction

Remarkable phenomena can be observed if an antiferromagnet is exposed to a uniform magnetic field. In the case of the one-dimensional spin-$\frac{1}{2}$ antiferromagnetic Heisenberg model

$$H = \tfrac{1}{2}\sum_{x=1}^{N} \boldsymbol{\sigma}(x)\boldsymbol{\sigma}(x+1) - B\sum_{x=1}^{N}\sigma_3(x) \tag{1.1}$$

these phenomena appear as field-dependent singularities in the static structure factors and are generated by 'soft modes' in the excitation spectrum. These gapless excitations lead to infrared singularities in the corresponding dynamical structure factors.

We expect that similar phenomena can be observed in other antiferromagnetic models as well, for example, in spin-1 models. The bilinear–biquadratic spin-1 model with Hamiltonian

$$H_{\mathrm{bb}}(\theta) = \cos\theta \sum_{x=1}^{N} \boldsymbol{S}(x)\boldsymbol{S}(x+1) + \sin\theta \sum_{x=1}^{N}[\boldsymbol{S}(x)\boldsymbol{S}(x+1)]^2 \tag{1.2}$$

interpolates between the spin-1 Heisenberg model with $\theta = 0$ and the $SU(3)$ symmetric Lai–Sutherland model with $\theta = \pi/4$. The first model ($\theta = 0$) is expected to have a gap according to Haldane's conjecture [1]. Moreover, it is not solvable in the sense of the Yang–Baxter equations. Therefore, most investigations of this model are restricted to a numerical

§ E-mail address: schmitt@wpts0.physik.uni-wuppertal.de
‖ E-mail address: muetter@wpts0.physik.uni-wuppertal.de
¶ E-mail address: karbach@uriacc.uri.edu
+ On leave from: University of Wuppertal, 42097 Wuppertal, Germany.

0305-4470/96/143951+12$19.50

diagonalization of the Hamiltonian on small lattices. On the other hand, the Lai–Sutherland model is known to be critical (gapless) and solvable by means of the nested Bethe ansatz [2]. From this point of view it is the natural spin-1 extension of the spin-$\frac{1}{2}$ Heisenberg model.

Owing to its solvability, the response of the Lai–Sutherland model to external and internal fields can be studied on large systems as will be demonstrated in this paper. Our starting point is the Hamiltonian

$$H = H_0 - BS_3 + DS_3^{(2)} \tag{1.3}$$

where

$$H_0 = \sqrt{2}H_{\mathrm{bb}}(\pi/4) = \sum_{x=1}^{N-1}\{\boldsymbol{S}(x)\boldsymbol{S}(x+1) + [\boldsymbol{S}(x)\boldsymbol{S}(x+1)]^2\} \tag{1.4}$$

$$S_3 \equiv \sum_{x=1}^{N} S_3(x) \qquad \text{and} \qquad S_3^{(2)} \equiv \sum_{x=1}^{N}[S_3(x)]^2. \tag{1.5}$$

Periodic boundary conditions are used so that $\boldsymbol{S}(N+1) = \boldsymbol{S}(1)$. The $S_i(x)$ are spin-1 representations of the $SU(2)$ algebra. The operators S_3 and $S_3^{(2)}$ commute with the bilinear–biquadratic interaction H_0:

$$[H_0, S_3] = [H_0, S_3^{(2)}] = 0. \tag{1.6}$$

They take into account the coupling to an external magnetic field B and to a single site anisotropy D, which can also be interpreted as an internal crystal field.

Owing to the commutation relations (1.6) the Hamiltonian can be brought into block form. The ground states in these blocks can be classified by the 'magnetizations'

$$M \equiv M_B \equiv \frac{S_3}{N} \qquad \text{and} \qquad M_D \equiv \frac{S_3^{(2)}}{N}. \tag{1.7}$$

From the ground-state energies per site $\epsilon(M_B, M_D)$ we obtain the magnetization curves in analogy to the spin-$\frac{1}{2}$ case:

$$\frac{\partial\epsilon(M_B, M_D)}{\partial M_B} = B \qquad \text{and} \qquad \frac{\partial\epsilon(M_B, M_D)}{\partial M_D} = D. \tag{1.8}$$

The $SU(3)$ symmetry of the field-independent part H_0 becomes more apparent if we reformulate the nearest-neighbour coupling in terms of Gell-Mann matrices $\lambda_A(x)$, $A = 1, \ldots, 8$, the generators of the $SU(3)$ algebra:

$$\begin{aligned}\boldsymbol{S}(x)\boldsymbol{S}(x+1) + [\boldsymbol{S}(x)\boldsymbol{S}(x+1)]^2 - 1 &= P(x, x+1) \\ &= \tfrac{1}{3} + \tfrac{1}{2}\sum_{A=1}^{8}\lambda_A(x)\lambda_A(x+1).\end{aligned} \tag{1.9}$$

$P(x, y)$ is a permutation operator for spin-1 particles residing at sites x and y. Because of this form of H_0 the numbers N_+, N_-, N_0 of the three species $+1, -1, 0$ are conserved. Therefore, the ground-state energies per site $\epsilon = \epsilon(n_+, n_-, n_0)$ are equally well characterized by the densities $n_i = N_i/N$, $i = +, -, 0$ with the constraint $n_+ + n_- + n_0 = 1$. The partial derivatives

$$\frac{\partial\epsilon(n_+, n_-, n_0)}{\partial n_i} = \mu_i \qquad i = +, -, 0 \tag{1.10}$$

have to be interpreted as chemical potentials. For this reason model (1.3) is equivalent to a lattice gas model

$$H = \sum_{x=1}^{N} P(x, x+1) + N_+\mu_+ + N_-\mu_-. \tag{1.11}$$

Via an unitary transformation, the couplings of the external and internal fields in (1.3) can be expressed in terms of the Gell-Mann matrices λ_3 and λ_8:

$$B_3 \sum_{x=1}^{N} \lambda_3(x) + B_8 \sum_{x=1}^{N} \lambda_8(x). \tag{1.12}$$

They form the Cartan subalgebra of $SU(3)$. B_3 and B_8 can be expressed as linear combinations of B and D.

It was shown in [2] that the Hamiltonian H_0 is integrable by a nested Bethe ansatz. The ground-state energy and dispersion relations in the sector $n_+ = n_- = n_0 = \frac{1}{3}$ were computed by Sutherland. The magnetization curve $M = M(B, D = 0)$ in the absence of a single site anisotropy—i.e. for the Hamiltonian (1.3) with $D = 0$—was derived in [3, 4].

It is the purpose of this paper to explore the whole phase diagram in the B–D plane. The latter is presented in section 2 where we also study the magnetization along the phase boundaries. Section 3 is devoted to a discussion of the magnetization curves as a function of the crystal field D. In section 4 we concentrate on the $SU(3)$ phase where the densities n_i of the three species $i = +, -, 0$ are non-vanishing. Lines of constant densities are presented and parametrized by modified hypocycloides. Finally the more technical details concerning the solution of the Bethe ansatz equations and the proper choice of the Bethe quantum numbers are given in the appendix.

In a second paper, we will treat the dispersion curves in the various density sectors and the behaviour of the static and dynamical structure factors in the presence of external and internal fields.

2. The phase diagram in the B–D plane

Owing to the $SU(3)$ symmetry of the Lai–Sutherland model, the ground-state energies are symmetric in the densities n_+, n_-, n_0:

$$\epsilon(n_+, n_-, n_0) = \epsilon(n_-, n_+, n_0) = \epsilon(n_+, n_0, n_-). \tag{2.1}$$

We have computed these energies in every density sector for chains up to $N = 360$. Inverting (1.10), we see how the densities depend on the chemical potentials. The latter are related to the external field B and the crystal field D via

$$\mu_+ = D - B \qquad \mu_- = D + B \qquad \mu_0 = -2D \tag{2.2}$$

which implies that $\mu_+ + \mu_- + \mu_0 = 0$ as a consequence of $n_+ + n_- + n_0 = 1$.

Using the densities as order parameters we have constructed the complete phase diagram in the B–D plane at temperature $T = 0$. The latter is shown in figure 1.

The $SU(3)$ symmetry of the phase diagram becomes apparent if we introduce a 'mercedes' star coordinate system for the chemical potentials. The symmetry is perfect after the renormalization of the single site anisotropy D by a factor $\sqrt{3}$. This factor can be traced back to the element λ_8 of the Cartan subalgebra of $SU(3)$:

$$\lambda_8 = \frac{1}{\sqrt{3}} \begin{pmatrix} 1 & 0 & 0 \\ 0 & 1 & 0 \\ 0 & 0 & -2 \end{pmatrix}. \tag{2.3}$$

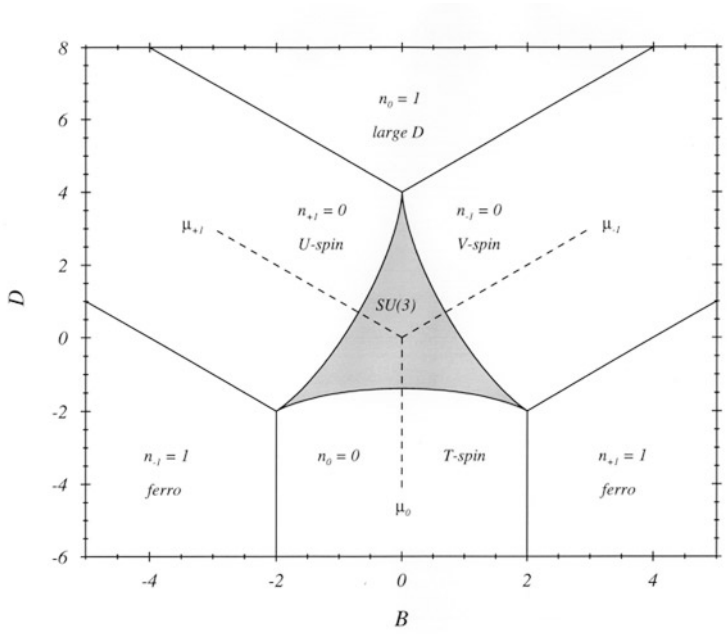

Figure 1. The phase diagram of the Lai–Sutherland model (1.3).

At the origin of the diagram ($B = D = 0$) one finds the ground state of the Lai–Sutherland model H_0 where the densities of the three species are equal. If we switch on the external or internal field the densities will change. The shaded region in figure 1 represents the $SU(3)$ phase. This is the domain where all three densities are non-vanishing. At the phases' boundary one of the densities becomes zero. For example, if we switch on the magnetic field along the line $D = 0$ we enter a $SU(2)$ region (at the point $B_c = 0.9415(8)$) in which the ground state contains only $+1$ or 0 particles. It is this special point of the phase boundary that was already found in [3, 4].

We distinguish three $SU(2)$ phases of this kind according to the three $SU(2)$ subalgebras of $SU(3)$. They are usually called the T-, V- and U-spin in elementary particle physics. In order to simplify notation we adopt these names. In the $SU(2)$ regions, model (1.3) becomes unitarily equivalent to the spin-$\frac{1}{2}$ Heisenberg model (1.1). For example, along the symmetry axis μ_0 ($B = 0$) for $D \leqslant -1.386(4)$ we find the non-magnetic ground state of (1.1). At the corner points of the $SU(3)$ phase at ($D = 4$, $B = 0$) and ($D = -2$, $B = \pm 2$) two species vanish simultanously and only one remains. The phases beyond these points are either of ferromagnetic character or consist of a state where only $S_3 = 0$ particles are present at every site. The $SU(2)$ domains are separated by straight lines from these regions where the symmetry is reduced to $U(1)$.

In order to parametrize the phase boundary B_c, D_c we introduce an angle in such a way that the corner points correspond to $\phi = 0, 2\pi/3$ and $4\pi/3$, respectively. Starting at $D_c = 4$, $B_c = 0$ clockwise such a parametrization has to obey the following symmetry relations,

$$B_c\left(\tfrac{2}{3}\pi \pm \phi\right) = \tfrac{1}{2}[D_c(\phi) \mp B_c(\phi)] \qquad D_c\left(\tfrac{2}{3}\pi \pm \phi\right) = -\tfrac{1}{2}[D_c(\phi) \pm 3B_c(\phi)] \tag{2.4}$$

together with $B_c(2\pi - \phi) = -B_c(\phi)$ and $D_c(2\pi - \phi) = D_c(\phi)$. These constraints are satisfied by the Fourier series

$$\begin{aligned} B_c(\phi) &= \sum_{k=0}^{\infty} \{h_{3k+1} \sin[(3k+1)\phi] - h_{3k+2} \sin[(3k+2)\phi]\} \\ D_c(\phi)/\sqrt{3} &= \sum_{k=0}^{\infty} \{h_{3k+1} \cos[(3k+1)\phi] + h_{3k+2} \cos[(3k+2)\phi]\} \end{aligned} \tag{2.5}$$

with unknown Fourier coefficients h_i. The intervals $[0, 2\pi/3]$, $[2\pi/3, 4\pi/3]$ and $[4\pi/3, 2\pi]$ for the angle ϕ correspond to the boundary between the $SU(3)$ domain and the V-spin, T-spin and U-spin region, respectively.

It should be noted that a good approximation of the phase boundary is already achieved with the $k = 0$ contribution (a hypercycloide) in the expansion (2.5). Within numerical accuracy, the data of a ring with $N = 360$ are reproduced correctly by means of the parametrization:

$$\begin{aligned} B_c(\phi) &= h_1 \sin\phi - h_2 \sin 2\phi + h_4 \sin 4\phi \\ D_c(\phi)/\sqrt{3} &= h_1 \cos\phi + h_2 \cos 2\phi + h_4 \cos 4\phi \end{aligned} \tag{2.6}$$

where $h_1 = 1.555(5)$, $h_2 = 0.765(5)$ and $h_4 = -0.011(5)$.

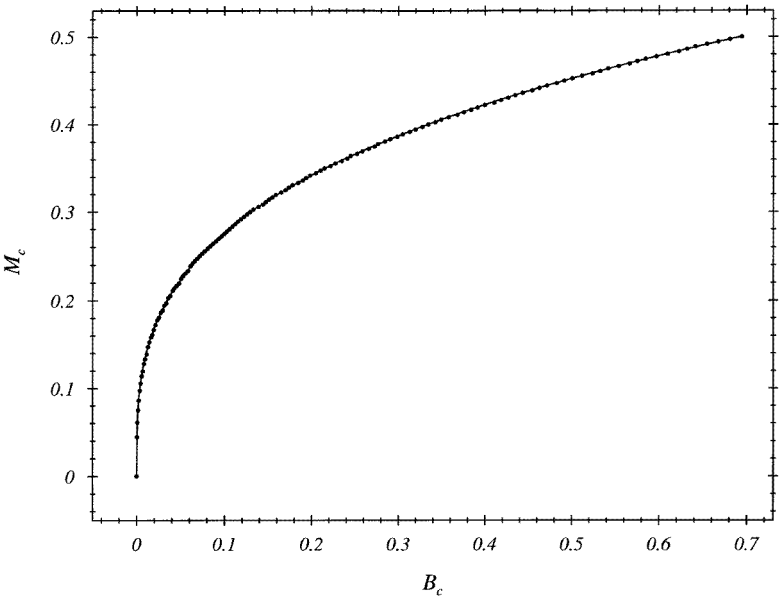

Figure 2. The magnetization $M_c(\phi)$ plotted against $B_c(\phi)$ along the phase boundary for $0 \leqslant \phi \leqslant \pi/3$. The full curve represents equation (2.7).

We have also calculated the magnetization $M_c(\phi)$ along the phase boundary for $0 \leqslant \phi \leqslant \pi/3$. As can be seen from figures 2 and 3, a fairly good description is given by

$$M_c(\phi) = \frac{1}{2}\left(\frac{B_c(\phi)}{B_c(\pi/3)}\right)^{0.305(5)} = \frac{1}{2}\left(\frac{D_c(0) - D_c(\phi)}{D_c(0) - D_c(\pi/3)}\right)^{0.475(5)} \tag{2.7}$$

where $D_c(0) = 4$ and $D_c(\pi/3) = B_c(\pi/3) = 0.693(2)$.

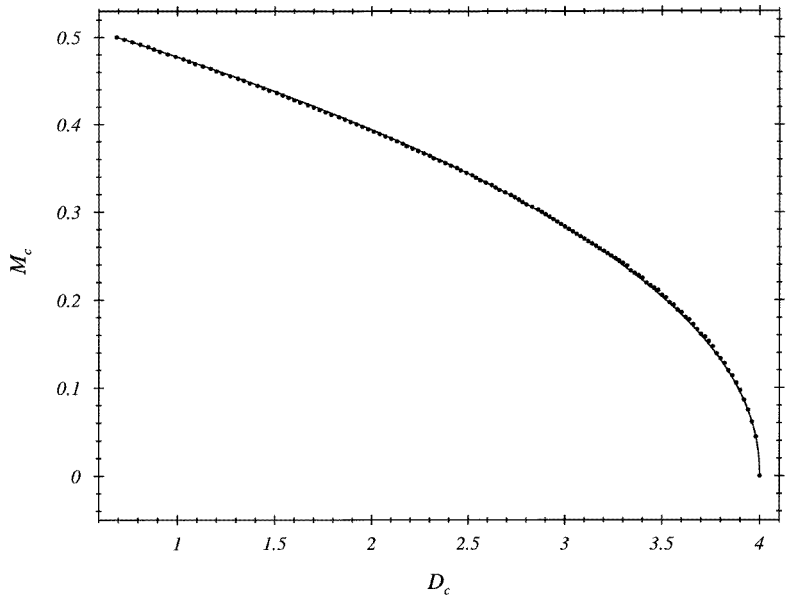

Figure 3. The magnetization $M_c(\phi)$ plotted against $D_c(\phi)$ along the phase boundary for $0 \leqslant \phi \leqslant \pi/3$. The full curve represents equation (2.7).

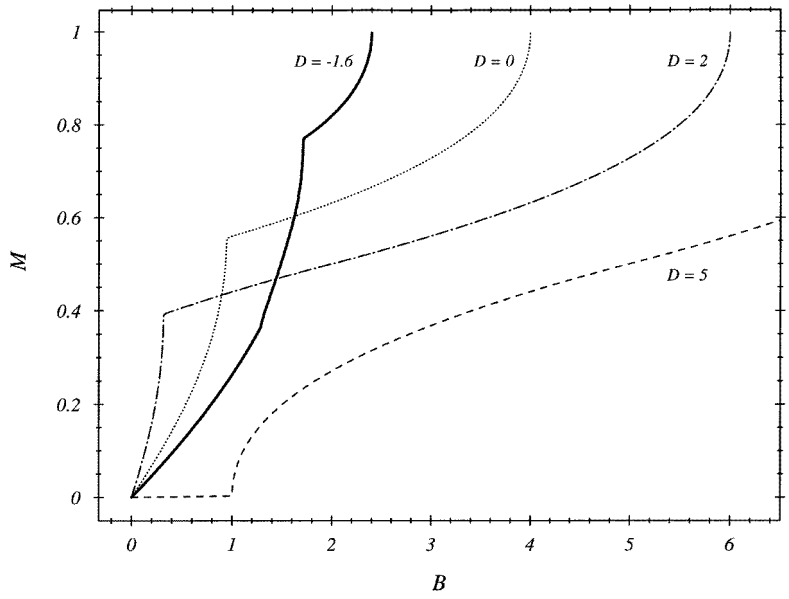

Figure 4. Magnetization curves of the Lai–Sutherland model for $D = -1.6, 0, 2$ and 5. The transition point from the $SU(3)$ phase to the V-spin phase varies with D according to equation (2.6). For $-2 < D < -1.386(4)$ a second transition point between the T-spin phase and the $SU(3)$ phase enters the scene.

3. Magnetization curves

From the densities $n_a(\mu_+, \mu_-, \mu_0)$ we get the magnetization curves $M = M(B, D)$ for fixed values of D. The latter are shown in figure 4 for $D = -1.6, 0, 2, 5$. In these curves

one observes discontinuities in the slopes at those magnetic fields where the system passes the phase boundaries in figure 1.

It is convenient to distinguish the following regimes.

(i) $D_c(2\pi/3) = -2 < D < -2D_c(\pi/3) = -1.386(4)$. At $B = 0$ we start in the T-spin phase. The magnetization curve is identical to that of the $SU(2)$ spin-$\frac{1}{2}$ model (1.1) up to a normalization factor of 2. At $B_{c1}(\phi_1)$ with $2\pi/3 < \phi_1 < \pi$ we enter the $SU(3)$ phase. In the $D = -1.6$ curve of figure 4 this point occurs at $B = 1.28$ and $M = 0.36$. Here the slope of the magnetization curve changes discontinuously. At a magnetic field $B_{c2}(\phi_2) > B_{c1}$ with $\pi/3 < \phi_2 < 2\pi/3$ we leave the $SU(3)$ phase and enter the V-spin domain where the magnetization curve is again of $SU(2)$ type.

(ii) $-2D_c(\pi/3) = -1.386(4) \leqslant D \leqslant 4$. At $B = 0$ we start in the $SU(3)$ phase which we leave at $B = B_c(D)$, where we enter the V-spin phase. The critical field $B_c(D)$ and the corresponding magnetization $M_c(D)$ decrease with increasing values of D. There is a discontinuity in the slope of the magnetization curve at the transition point. Above $B_c(D)$ the magnetization curve is of $SU(2)$ type. The special case $D = 0$ has been treated previously in [3, 4].

(iii) $D > 4$. At $B = 0$ we start in the large-D phase, where the magnetization vanishes. There is a gap in the exitation spectrum and, therefore, a finite magnetic field $B = D - 4$ is needed to reach a magnetic state. At this value of B, we pass to the V-spin phase. Here the magnetization curve is again of $SU(2)$ type.

The singular behaviour of the magnetization curve in the $SU(3)$ phase, if one approaches the boundary to the V-spin domain, is well described by

$$1 - \frac{M}{M_c(D)} = -\left(1 - \frac{B}{B_c(D)}\right)^{\alpha} \tag{3.1}$$

where the critical exponent

$$\alpha = 0.52(2) \tag{3.2}$$

appears to be independent of D.

The saturation field $B_s(D)$, which is necessary for magnetization $M = 1$, can be read off figure 1:

$$B_s(D) = \begin{cases} 2 & \text{for } D \leqslant -2 \\ D + 4 & \text{for } D > -2. \end{cases} \tag{3.3}$$

The approach to this limiting value in the V-spin or T-spin phase is governed by the square root singularity of $SU(2)$ type:

$$M - 1 \sim \sqrt{B_s - B}. \tag{3.4}$$

A complete view on the B- and D-dependence of the magnetization $M(B, D)$ is presented in figure 5.

4. Lines of constant density

The inherent $SU(3)$ symmetry of the Lai–Sutherland model in external and internal fields becomes apparent in a plot of curves of constant density. The latter is given in figure 6.

Let us start with the case $n_i = \frac{1}{2}$. This curve is represented by the dashed curve, which meets the boundaries of the $SU(3)$ phase at three points. At these points the coordinate

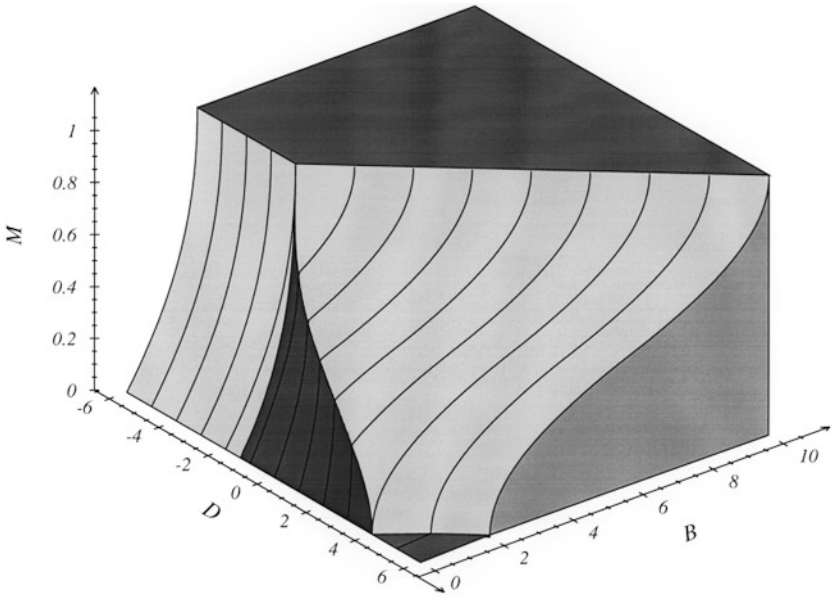

Figure 5. The magnetization curves of the Lai–Sutherland model. The different phases of the model are coloured differently. From left to right they are the T-spin-, $SU(3)$-, V-spin- and 'large D'-phase. The top of the figure is the ferromagnetic phase with $n_+ = 1$.

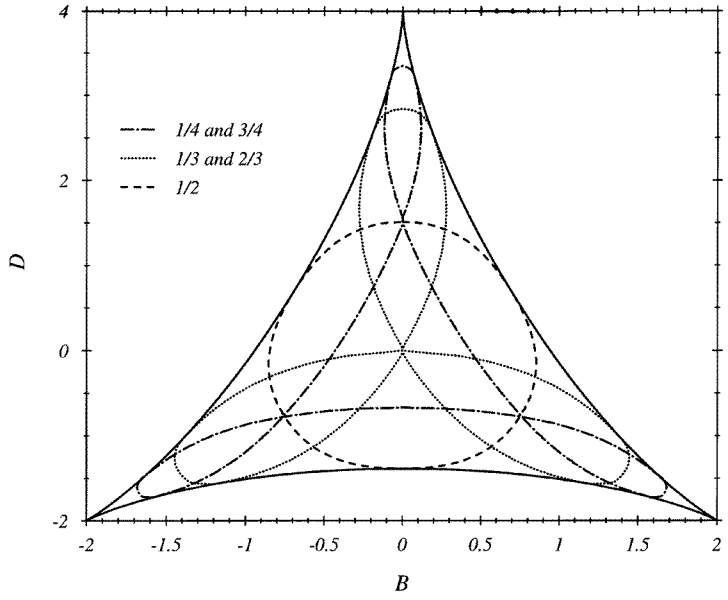

Figure 6. Curves of constant density in the $SU(3)$ phase. Which curve belongs to which density n_a, $a = +, -, 0$ is explained in the text.

axes for the chemical potentials μ_i, $i = +, -, 0$, cross the $SU(3)$-phase boundary. The μ_i-axes divide the dashed curve into three sections: we have $n_0 = \frac{1}{2}$, $n_+ = \frac{1}{2}$ and $n_- = \frac{1}{2}$ between the $\mu_+\mu_-$, $\mu_-\mu_0$ and $\mu_0\mu_+$ axes, respectively.

Curves of constant density with $n_i = \frac{1}{3}, \frac{2}{3}$ have 'clover' form and are represented by the dotted curve in figure 6. The curve is divided into six branches by the six tangential points with the $SU(3)$ phase boundary. Starting at the $SU(3)$ symmetric point $D = B = 0$ and switching on $D > 0$ as well as $B > 0$ we enter the upper right part of the $SU(3)$ domain. Here we have $n_+ = \frac{1}{3}$ along the dotted curve until we reach the $SU(3)$ V-spin boundary. Following the dotted curve further in the same sense of circulation means moving along the curve $n_0 = \frac{2}{3}$ until we reach the $SU(3)$ U-spin boundary. Afterwards we follow the curves along $n_- = \frac{1}{3}$ (thereby moving again through the origin), $n_+ = \frac{2}{3}$, $n_0 = \frac{1}{3}$, $n_- = \frac{2}{3}$ and finally $n_+ = \frac{1}{3}$. Therefore, after a full revolution we get back (now for the third time) to the $SU(3)$ symmetric point. The curves of constant density with $n = \frac{1}{4}, \frac{3}{4}$ in figure 6 have to be interpreted in the same sense.

In general, it is useful to combine sections with $n < \frac{1}{2}$ fixed and $1 - n$ fixed in order to obtain closed and symmetric curves, which can be parametrized as $B_n(\phi)$, $D_n(\phi)$ by the angle ϕ, introduced already for the parametrization of the phase boundary. The symmetry constraints are satisfied by a Fourier series of type (2.5). Moreover, it turns out that the truncated series

$$\begin{aligned} B_n(\phi) &= h_1(n)\sin\phi - h_2(n)\sin 2\phi + h_4(n)\sin 4\phi \\ D_n(\phi)/\sqrt{3} &= h_1(n)\cos\phi + h_2(n)\cos 2\phi + h_4(n)\cos 4\phi \end{aligned} \tag{4.1}$$

reproduces the numerical data with great accuracy. Indeed, the parametrization of the phase boundary (2.6) can be interpreted as a curve of constant density $n = 0$. The coefficients $h_i(n)$, $i = 1, 2, 4$, are given in table 1. For $n \to \frac{1}{2}$, $h_1(n)$ drops to zero while the $h_4(n)$ becomes more important. At $n = \frac{1}{2}$ the periodicity of the curve reduces from 2π to π.

Table 1. The coefficents $h_i(n)$.

n	$h_1(n)$	$h_2(n)$	$h_4(n)$
0	1.555(5)	0.765(5)	−0.011(5)
$\frac{1}{4}$	1.144(8)	0.786(8)	0.000(8)
$\frac{1}{3}$	0.820(5)	0.804(5)	0.016(5)
$\frac{1}{2}$	0.000(5)	0.837(5)	0.037(5)

For general $0 < n < \frac{1}{2}$ the coefficents $h_1(n)$, $h_2(n)$ and $h_4(n)$ can be calculated from the values of $D_n(\phi)$ on the symmetry axes at $\phi = 0, \pi$ and an intermediate angle $0 < \phi_n < \pi$, where $B_n(\phi_n) = 0$:

$$\begin{aligned} h_1(n) &= \frac{D_n(0) - D_n(\pi)}{2\sqrt{3}} \qquad h_2(n) + h_4(n) = \frac{D_n(0) + D_n(\pi)}{2\sqrt{3}} \\ h_2(n) - h_4(n) &= \frac{D_n(\phi_n)\sin\phi_n}{\sqrt{3}\sin 3\phi_n}. \end{aligned} \tag{4.2}$$

Here we have to exclude the special case $n = \frac{1}{3}$ which corresponds to $\phi_n = \pi/3$. For given $D_n(0)$, $D_n(\phi_n)$ and $D_n(\pi)$ the angle ϕ_n follows from

$$2D_n(\phi_n)\cos\phi_n = D_n(0)(\cos 3\phi_n + 1) + D_n(\pi)(\cos 3\phi_n - 1). \tag{4.3}$$

The values $D_n(\phi)$ for $\phi = 0, \phi_n, \pi$ can be determined from the density $n_0(D, B = 0)$ at vanishing magnetic field. The dependence on the single site anisotropy D is shown in

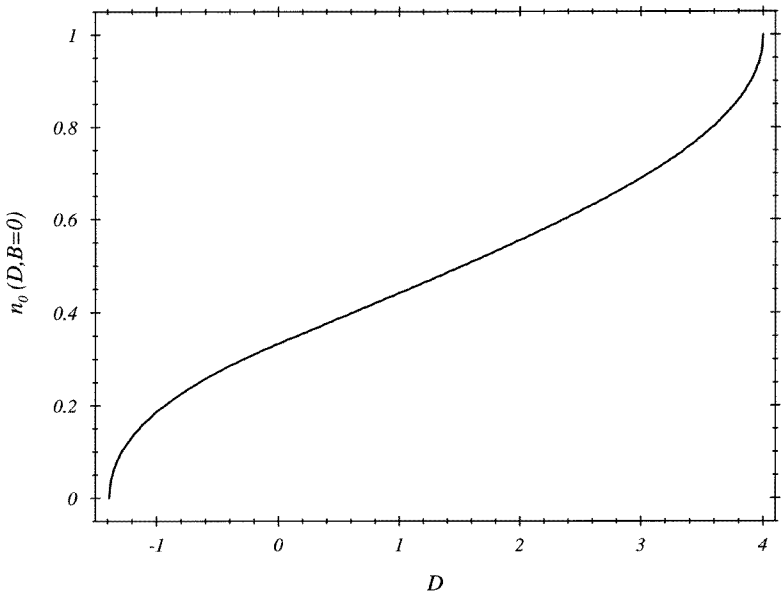

Figure 7. The variation of the density n_0 along the symmetry axis $B = 0$ plotted against the internal field D.

figure 7. It can be approximately parametrized as follows:

$$n_0(D, B=0) = \begin{cases} \dfrac{1}{3}\left[1 + \dfrac{D}{2D_c(\pi/3)}\right]^{\alpha} & \text{for } -2D_c(\pi/3) \leqslant D \leqslant 0 \\ \frac{1}{3} + \gamma D & \text{for } 0 \leqslant D \leqslant D_{\frac{1}{2}}(0) \\ 1 - \dfrac{1}{2}\left[\dfrac{4-D}{4-D_{\frac{1}{2}}(0)}\right]^{\beta} & \text{for } D_{\frac{1}{2}}(0) \leqslant D \leqslant 4. \end{cases} \tag{4.4}$$

The parameters were found to be

$$\gamma = 0.110(5) \qquad D_{\frac{1}{2}}(0) = 1.515(5) \qquad \alpha = 0.460(5) \qquad \beta = 0.520(5). \tag{4.5}$$

The three regions for D in equation (4.4) correspond to the density intervals $0 \leqslant n_0 \leqslant \frac{1}{3}$, $\frac{1}{3} \leqslant n_0 \leqslant \frac{1}{2}$ and $\frac{1}{2} \leqslant n_0 \leqslant 1$, respectively. Evaluating the inverse of (4.4)—i.e. $D = D(n_0, B = 0)$—at $n_0 = n, 1-n$ and $1-2n$, we get the values $D_n(\phi)$ for $\phi = 0, \phi_n, \pi$ which enter on the right-hand-side of (4.2):

$$\begin{aligned} D_n(\phi = 0) &= D(n_0 = 1 - n, B = 0) \\ D_n(\phi = \phi_n) &= \begin{cases} D(n_0 = 1 - 2n, B = 0) & \text{for } 0 < n < \frac{1}{3} \\ D(n_0 = n, B = 0) & \text{for } \frac{1}{3} < n < \frac{1}{2} \end{cases} \\ D_n(\phi = \pi) &= \begin{cases} D(n_0 = n, B = 0) & \text{for } 0 < n < \frac{1}{3} \\ D(n_0 = 1 - 2n, B = 0) & \text{for } \frac{1}{3} < n < \frac{1}{2}. \end{cases} \end{aligned} \tag{4.6}$$

It should be noted that the dependence of the densities $n_i(B, D)$, $i = +, -, 0$, on the external and internal fields can be reconstructed completely from the curve $n_0 = n_0(D, B = 0)$ making use of the approach outlined in equations (4.1)–(4.6).

5. Conclusions

In this paper we have investigated the solvable $SU(3)$ spin-1 Lai–Sutherland model in the presence of a magnetic field and a single site anisotropy. The phase diagram at zero temperature is divided into seven regimes. In the $SU(3)$ domain all three densities n_+, n_-, n_0 are non-vanishing. In the three $SU(2)$ domains, called U-, V- and T-spin phase, one species is absent. In the three $U(1)$ domains two species are absent. The internal symmetry of the model manifests itself in a rotation symmetry by an angle $2\pi/3$ in the B–D plane. The phase boundary can be well parametrized by a modified hypocycloide. A generalization of this curve also allows for an accurate description of the curves of constant density inside the $SU(3)$ phase. Therefore, the full phase diagram could be reconstructed in principle from a detailed knowledge of the variation of the n_0 density along the symmetry axis $B = 0$. We have also studied the dependence of the magnetization curves from the crystal field. The critical exponent which describes the singularity in the susceptibility $\chi = \partial M_B/\partial B$ at the phase transition point from the $SU(3)$ phase to the V-spin phase seems to be 0.52, independent of D. The transition effectively reduces the spin quantum number from 1 to $\frac{1}{2}$. For $D < -1.386(4)$ we find a particularly interesting situation: switching on the magnetic field one first starts in the T-spin phase, then enters the $SU(3)$ phase, which again is left to enter the V-spin phase. Therefore, we find here two transitions and two discontinuities in the slope of the magnetization curve. It would be interesting if one could observe such phenomena in an experiment on a quasi-one-dimensional spin-1 system at low temperature.

In a forthcoming publication we will investigate the static and dynamical structure factors of the spin-1 Lai–Sutherland model in the presence of an external magnetic field B and an internal crystal field D. Zero frequency exitations ('soft modes') are of special interest; in particular the B and D dependence of the soft mode momenta and of the exponents for the infrared singularities. The comparison with the spin-$\frac{1}{2}$ antiferromagnetic Heisenberg model should reveal interesting differences as well as similarities of one-dimensional quantum spin chains with integer or half-integer spin.

Acknowledgment

MK gratefully acknowledges support by the Max Kade Foundation.

Appendix. The Bethe ansatz equations

The $SU(n)$ Lai–Sutherland model is integrable by the nested Bethe ansatz. In the $SU(3)$ case, which corresponds to the spin-1 model equation (1.3), the number of Bethe ansatz equations is two ($n-1$ in general). Assuming that the three conserved quantum numbers N_a, N_b, N_c with $a, b, c \in \{-, 0, +\}$ are ordered as $N_a \leqslant N_b \leqslant N_c$ (with $N_a + N_b + N_c = N$), the two Bethe ansatz equations read:

$$N \arctan x_i = \pi J_i + \sum_{j=1}^{N_a+N_b} \arctan\left(\frac{x_i - x_j}{2}\right) - \sum_{\beta=1}^{N_a} \arctan(x_i - y_\beta) \tag{A.1}$$

$$0 = \pi I_\alpha + \sum_{j=1}^{N_a+N_b} \arctan(x_j - y_\alpha) + \sum_{\beta=1}^{N_a} \arctan\left(\frac{y_\alpha - y_\beta}{2}\right) \tag{A.2}$$

for $i = 1, \ldots, N_a + N_b$ and $\alpha = 1, \ldots, N_a$.

The *a priori* unknown Bethe quantum numbers J_i and I_α are integers or half-integers. These quantum numbers characterize an eigenstate of the Hamiltonian (1.3). The roots x_i of equations (A.1) and (A.2) determine the energy per site:

$$\epsilon(n_a, n_b, n_c) = 1 - \frac{4}{N} \sum_{j=1}^{N_a+N_b} \frac{1}{1+x_j^2} - B(n_+ - n_-) + D(n_+ + n_-). \tag{A.3}$$

The momentum of the eigenstate is given by the sum of the Bethe quantum numbers

$$p = \frac{2\pi}{N} \left(\sum_{i=1}^{N_a+N_b} J_i + \sum_{\alpha=1}^{N_a} I_\alpha \right) + (N_a + N_b)\pi \mod 2\pi. \tag{A.4}$$

In the $SU(3)$ phase, chains of length $N \bmod(3) = 0$ behave differently from chains with $N \bmod(3) = 1, 2$. Similarly, in the $SU(2)$ phase, chains with N even or odd behave differently [8]. We have studied chains of length N which are multiples of six. By comparison of the solutions of the two Bethe ansatz equations (A.1) and (A.2) with the results of an exact diagonalization of chains up to $N = 18$ we have determined the systematics of the quantum numbers J_i and I_α. We found that the ground states in a given density sector are always given by a set of integers or half-integers with

$$J_{i+1} - J_i = 1 \quad \text{and} \quad I_{\alpha+1} - I_\alpha = 1. \tag{A.5}$$

The corresponding roots x_i and y_α are real. This distribution of the quantum numbers for the ground states could be expected from the knowledge of the Bethe ansatz solutions of the $SU(2)$ spin-$\frac{1}{2}$ Heisenberg model [5–7]. A remarkable difference to the spin $\frac{1}{2}$ case is that the quantum numbers I_α are, in general, not distributed symmetrically around zero. Nevertheless, we found out that with increasing N_a the symmetry in the distribution of the I_α increases. Therefore, deep inside the $SU(3)$ phase both quantum numbers J_i and I_α are distributed symmetrically around zero.

References

[1] Haldane F D M 1983 *Phys. Lett.* **93A** 464; 1983 *Phys. Rev. Lett.* **50** 1153
[2] Lai J K 1974 *J. Math. Phys.* **15** 1675
Sutherland B 1975 *Phys. Rev.* B **12** 3795
Uimin G V 1970 *JETP Lett.* **12** 225
[3] Parkinson J B 1989 *J. Phys.: Condens. Matter* **1** 6709
[4] Kiwata H 1995 *J. Phys.: Condens. Matter* **7** 7991
[5] Bethe H A 1931 *Z. Phys.* **71** 205
[6] Yang C N and Yang C P 1966 *Phys. Rev.* **150** 321
[7] Griffiths R B 1964 *Phys. Rev.* **133** A768
[8] Karbach M and Mütter K-H 1995 *J. Phys. A: Math. Gen.* **28** 4469